Proceedings of the 7th International Conference on Gas Hydrates (ICGH 2011),
Edinburgh, Scotland, United Kingdom, July 17-21, 2011.

CONSTRAINING THE GLOBAL INVENTORY OF METHANE HYDRATE IN MARINE SEDIMENTS

Klaus Wallmann
Ewa Burwicz
Lars Ruepke
Matthias Marquardt
Elena Pinero
Matthias Haeckel
Christian Hensen

IFM-GEOMAR
Leibniz Institute of Marine Sciences
Wischhofstrasse 1-3, 24148 Kiel
Germany

ABSTRACT

The accumulation of methane hydrate in marine sediments is basically controlled by the accumulation of particulate organic carbon at the seafloor, the kinetics of microbial organic matter degradation and methane generation in marine sediments, the thickness of the gas hydrate stability zone (GHSZ), the solubility of methane in pore fluids within the GHSZ and the ascent of deep-seated pore fluids and methane gas into the GHSZ. Our present knowledge on these controlling factors is discussed and new estimates of global sediment and methane fluxes are presented. A new transport-reaction model is applied at a global grid defined by these up-dated parameter values. The model yields an improved and better constrained estimate of the global inventory of methane gas hydrates in marine sediments (3000 ± 2000 Gt of methane carbon).

Keywords: methane hydrates, marine sediments, global inventory, transport-reaction modeling

INTRODUCTION

The global abundance of methane hydrate in marine sediments is still poorly constrained. Estimates are based on extrapolation of field data [1, 2] and geochemical transport-reaction modeling [3-5]. They range over three orders of magnitude (500 – 57 000 Gt C) and a clearly constrained consensus value has not emerged over the past decades. This is a major draw-back for hydrate research since the resource potential and the possible impact of methane hydrates on past and future climate change can not be evaluated without a well constrained estimate of global methane hydrate abundance. Models and observations clearly show that methane hydrate formation is basically controlled by the following key parameters: 1. accumulation rate of particulate organic carbon at the seafloor; 2. kinetics of microbial organic matter degradation and methane generation in marine sediments; 3. thickness of the gas hydrate stability zone (GHSZ); 4. solubility of methane in pore fluids within the GHSZ; 5. ascent of deep-seated pore fluids and methane gas into the GHSZ. In the following, we will present the state-of-the-art and discuss the major unknowns with respect to the key parameters listed above. Based on this evaluation, a new geochemical transport-model is applied to constrain the global gas hydrate inventory in marine sediments.

Accumulation of particulate organic carbon at the seafloor

Methane production and methane hydrate formation are fueled by the accumulation of particulate organic carbon (POC) at the seabed. Modeling studies thus reveal a positive correlation between POC and gas hydrate accumulation rates [6]. The POC accumulation rate at the seabed is calculated as:

$$A_{POC} = POC/100\ d_S\ (1-\Phi)\ w \qquad (1)$$

where POC is the concentration of organic carbon in surface sediments (in wt-%), d_S is the density of dry solids (in g cm^{-3}), Φ is porosity, w is burial velocity (in cm yr^{-1}) and A_{POC} is the accumulation rate (in g cm^{-2} yr^{-1}). POC concentrations have been measured at several thousand sites covering most depositional areas at the seabed (s. Fig. 1). The data have been compiled and evaluated to produce global maps of POC concentrations in marine surface sediments [7-9].

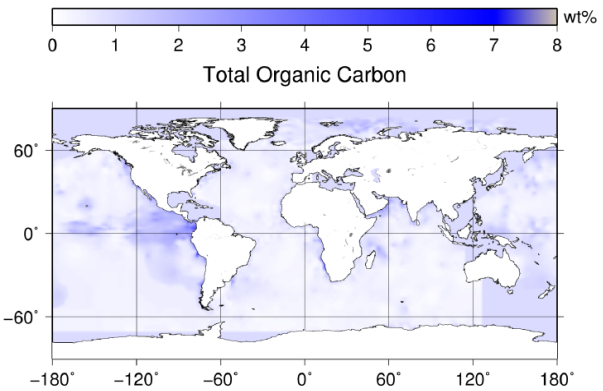

Figure 1 Concentration of particulate organic carbon in Holocene surface sediments [9]

Burial velocities have also been determined at several hundred locations for Holocene surface sediments. However, a global compilation of data covering all ocean basins and margins is currently not available. The published data clearly show that burial velocities are high on the continental shelf and decrease with increasing water depth (see Fig. 2).

Most of the sediments accumulating at the seabed are derived from the continents. Moreover, the solid remains of marine plankton (carbonate, biogenic opal) are deposited at the deep-sea floor as pelagic sediments. The global accumulation rate of sediments at the modern seafloor amounts to about 20 x 10^{15} g yr^{-1}. This number is derived considering the transport of riverine, eolian and ice-rafted sediments to the ocean, the accumulation of neritic carbonates at the continental shelf and the accumulation of pelagic sediments at the deep-sea floor (s. Table 1).

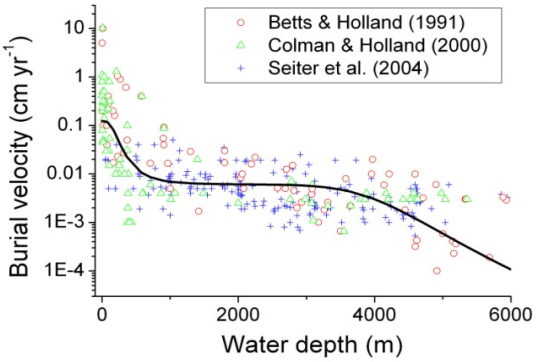

Figure 2 Burial velocity (w) in Holocene surface sediments. Data are taken from [10], [11] and [7]. The solid trend line is defined by Eq. (2).

	Flux	Reference
Riverine particles	14.0	[12]
Ice-rafted particles	2.9	[13]
Dust	0.45	[14]
Shelf carbonate	1.0	[15]
Pelagic carbonate	1.0	[16]
Biogenic opal	0.27	[17]
Total	**19.62**	

Table 1 Global accumulation rates at the seafloor (in 10^{15} g yr^{-1}). The listed values are valid for the pre-human Holocene.

The depth-distribution of sediment accumulation (Fig. 2) and the global accumulation rate (Tab. 1) can be used to constrain parameter values of a logistics equation defining the burial velocity as function of water depth (z in m):

$$w = \frac{w_1}{1+\left(\frac{z}{z_1}\right)^{c1}} + \frac{w_2}{1+\left(\frac{z}{z_2}\right)^{c2}} \qquad (2)$$

with w_1 = 0.117 cm yr^{-1}, w_2 = 0.006 cm yr^{-1}, z_1 = 200 m, z_2 = 4000 m, c_1 = 3, c_2 = 10. Eq. (2) yields a global sediment accumulation of 19.6 x 10^{15} g yr^{-1} for Φ = 0.8 and d_S = 2.5 g cm^{-3} when applied to

the global bathymetric data set given by Menard and Smith [18]. The equation predicts that most of the global sedimentation takes place on the continental shelf (14.1 x 10^{15} g yr^{-1} at 0 – 200 m water depth). These estimates are consistent with other data recently presented by Baturin [19]. Baturin derived a total sedimentation rate of 18.9 x 10^{15} g yr^{-1} with a shelf and upper slope contribution of 13.6 x 10^{15} g yr^{-1}. Sediments accumulating at shallow water depths (<200 m) can not contribute to gas hydrate accumulation since marine methane hydrates are only formed at significantly higher pressures and water depths. During the Holocene, the accumulation of methane hydrates is thus severely limited by the continental shelf acting as a trap for the continental sediment input.

However, the Holocene sedimentation pattern is not representative for the Quaternary. During glacial sea-level low-stands large continental shelf areas were exposed and eroded. Shelf sediments were thus displaced and transported down-slope towards the gas hydrate stability zone under glacial conditions such that most of the riverine particle input has been ultimately deposited at the continental slope and rise over the late Quaternary. It usually takes several million years to accumulate gas hydrates via microbial POC degradation within the GHSZ. Holocene sedimentation patterns can thus not be applied to derive a reasonable estimate of global gas hydrate abundance.

Physical erosion and terrigenous sedimentation are strongly affected by climatic conditions and orogenesis. Global rates of erosion and terrigenous sedimentation have been reconstructed over the last 150 million years (s. Fig. 3). These data show that the Quaternary is characterized by extremely high sedimentation rates favoring the formation of gas hydrates [20]. Interestingly, the early Cenozoic and the PETM (55 million years b. p.) are marked by very low sedimentation rates. It is thus likely that the global gas hydrate inventory increased significantly over the last 10 million years and was much lower than today during most of the Cenozoic and Mesozoic.

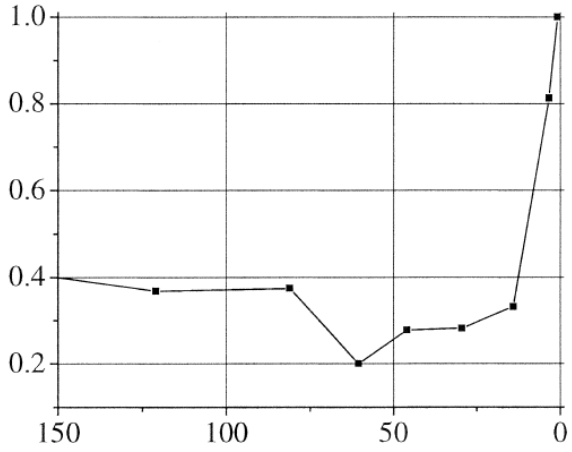

Figure 3 Change in the global rate of terrigenous sedimentation over the past 150 million years (Myr). Age in Myr is plotted as x-axis while the y-axis gives the global sedimentation rate normalized to the Holocene value [20].

Microbial methane formation in marine sediments

Stable carbon isotope data show that most methane hydrates are formed from biogenic methane produced by the anaerobic degradation of organic matter in the deep marine biosphere. It is thus important to understand the mechanisms and kinetics of organic matter degradation and microbial methane formation in the marine subsurface.

Organic matter deposited at the seabed is degraded by microorganisms and other benthic biota living at the seafloor and in marine sediments. Oxygen is used as terminal electron acceptor by benthic animals and aerobic bacteria. The remaining organic matter is degraded by anaerobic bacteria using dissolved nitrate and manganese (+IV) and iron (+III) minerals as oxidizing agents. These additional electron acceptors are usually consumed within the bioturbated surface layer (0 – 10 cm sediment depth). Field data show that only a small fraction of the POC raining to the seafloor is buried below 10 cm depth (s. Fig. 4). The data reveal a marked contrast between fine-grained continental margin and deep-sea sediments. While at continental margins about 10 % of the POC raining to the seabed is conserved and buried below 10 cm sediments, this fraction is reduced to about 1 % at the deep-sea floor. Due to the very low preservation of POC in open ocean environments, gas hydrates are usually not found

in pelagic sediments but only at continental margins where a significant POC fraction is buried and therefore available for microbial methane formation in the deep subsurface.

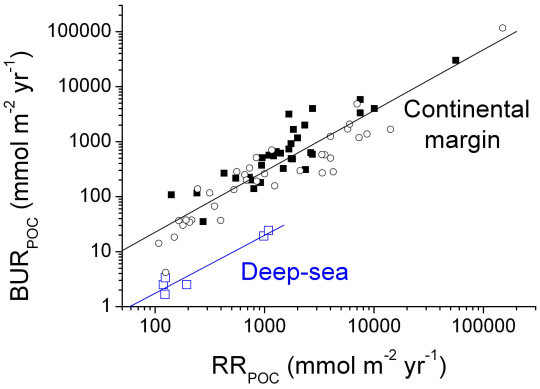

Figure 4 Burial of particulate organic carbon (BUR_{POC}) below 10 cm sediment depth as function of organic carbon rain rate to the seafloor (RR_{POC}). Open black circles indicate data from continental margin sites with oxygen-bearing bottom waters (O_2 >20 µM). Solid black squares represent continental margin sediments covered with oxygen-depleted bottom waters (O_2 <20 µM). Continental margin data are taken from various sources [10, 21-24]. Blue open squares indicate mean values averaged over major ocean basins [25]. Solid lines define the trends observed in margin and deep-sea sediments [26].

The buried POC is further degraded by anaerobic bacteria and archaea using dissolved sulfate as electron acceptor. Methane generation starts below the depth of sulfate penetration. Several steps are needed before methane is finally produced as stable end product of anaerobic microbial POC degradation. In a first step, biogenic polymers are hydrolyzed and converted into monomers. The monomers (sugars, amino acids, lipids, etc.) are then fermented into CO_2, H_2 and a number of organic acids. Methane is finally formed by methanogenic microorganisms converting CO_2 and H_2 into methane:

$$CO_2 + H_2 \Rightarrow CH_4 + H_2O \qquad (3)$$

The stoichiometry of the overall process of organic matter degradation and methanogenesis is given by the following reaction:

$$C(H_2O) \Rightarrow CH_4 + CO_2 \qquad (4)$$

where $C(H_2O)$ represents the sedimentary POC. Eq. (4) does not imply that methane is directly formed by POC degradation. It rather defines the substrate and the final products. The intermediate steps including fermentation and CO_2 reduction with H_2 are included in the overall stoichiometry [27].

The key questions that need to be answered to estimate the global rate of methane formation may be formulated as: How much POC is reaching the methanogenic zone and how much of that POC can be microbially converted into methane? To answer these questions not only the POC burial rates but also the down-core changes in POC reactivity need to be defined. Since more than three decades marine geochemists and microbiologists have shown that the POC reactivity decreases strongly with sediment age and depth. In his classical paper on POC degradation kinetics in marine sediments J. J. Middelburg showed that the down-core decrease in POC reactivity can be represented by the following equation [28]:

$$k_{age} = 0.16\ (age_0 + age)^{-0.95} \qquad (5)$$

where k_{age} is the age-dependent reactivity (in yr^{-1}) and age_0 is the initial age of POC (in yr). The equation was calibrated by a large number of rate measurements showing that the reactivity of POC decreases by more than 10 orders of magnitude going from fresh marine plankton to POC buried in ancient sediments. The overall trend was later confirmed by microbiologists studying the turnover of POC in the deep marine biosphere. The rate of POC degradation (R_{POC} in g g^{-1} yr^{-1}) is calculated as:

$$R_{POC} = -dC_{POC}/dt = k_{age}\ C_{POC} \qquad (6)$$

where C_{POC} is the POC concentration (in g C per g dry weight).

Equations (5) and (6) can be combined and solved to estimate the POC loss within the sulfate reduction zone and thereby the input of POC into the methanogenic zone. The fraction of POC reaching the methanogenic zone results as:

$$f_{MI} = \exp(3.2\ age_0^{1/20} - 3.2\ (t_{exp} + age_0)^{1/20}) \qquad (7)$$

where t_{exp} is the sulfate exposure time and f_{MI} is the concentration of POC in sediments reaching the methanogenic zone divided by the POC concentration in sediments buried below the bioturbated zone at 10 cm depth. The sulfate exposure time depends on sulfate penetration depth (z_S in m) and burial velocity (w in m yr^{-1}):

$$t_{exp} = (z_S\text{-}0.1)/w \qquad (8)$$

Burial velocities at the deep-sea floor typically range from 0.1 - 10 cm kyr^{-1} (s. Fig. 2) while sulfate penetrates usually more than 100 m into pelagic sediment. The sulfate exposure time in deep-sea sediments is thus typically larger than one million years and may reach values of up to 100 million years. Thus, less than 15 % of the POC buried below the bioturbated zone is reaching the methanogenic zone since more than 85 % of the POC is consumed in the overlying sediments (s. Fig. 5).

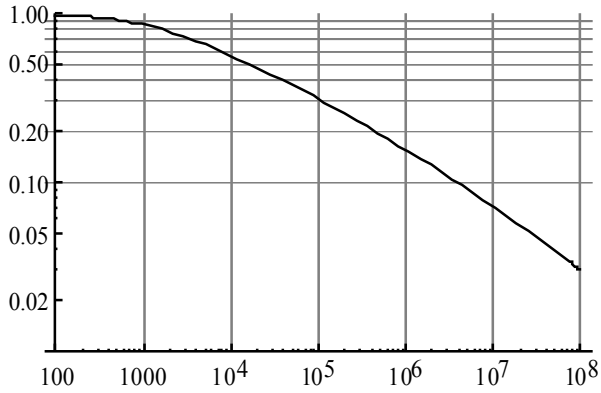

Figure 5 Fraction of buried POC entering the methanogenic zone (f_{MI}, y-axis) as function of sulfate exposure time (t_{exp} in yr, x-axis) as calculated from Eq. (7) for an initial age of age_0 = 1000 years

Sulfate dissolved in ambient pore fluids is typically consumed at 10 – 100 m sediment depth in most continental margin settings. The sulfate exposure time results as $t_{exp} = 10^4 – 10^6$ yr for burial velocities of 10 – 100 cm kyr^{-1} (s. Fig. 2). Thus, about 15 – 60 % of the buried POC is reaching the methanogenic zone in continental margin sediments.

The kinetics of microbial methane formation in marine sediments was studied in detail by Wallmann et al. [27]. Evaluating pore water and sediment data from the Sakhalin Slope and the Blake Ridge, the authors showed that the rate of methane formation within the methanogenic zone (R_{CH4} in g of methane carbon g^{-1} yr^{-1}) can be calculated as (Eq. 9):

$$R_{CH4} = -0.5\frac{dC_{POC}}{dt} = \frac{0.5\,K_C}{C_{CH4} + C_{DIC} + K_C} k_{age}\, C_{POC}$$

where K_C is an inhibition constant (K_C = 30 – 50 mM), C_{DIC} is the concentration of dissolved inorganic carbon in ambient pore fluids and C_{CH4} the dissolved methane concentration (in mM). This extension of the Middelburg model was subsequently tested and applied at a number of ODP drill sites in prominent gas hydrate provinces [6]. The evaluation of pore water profiles showed that kinetic equation (9) gives indeed a very good approximation of the down-core changes in microbial methane formation within the GHSZ. Eq. (9) can be solved to calculate the fraction of POC being converted into methane carbon within the methanogenic zone (Eq. 10):

$$f_M = 0.5\,(1 - \exp\left(\frac{20\,K_C\left(age_0^{\,1/20} - (t + age_0)^{1/20}\right)}{6.25\left(C_{CH4} + C_{DIC} + K_C\right)}\right)$$

where t is the residence time of sedimentary POC within the methanogenic zone while f_M is the ratio between microbially produced methane carbon and POC entering the methanogenic zone from above.

Considering the low sedimentation rates and high sulfate exposure times, typical deep-sea sediments entering the methanogenic zone have an initial age of $age_0 > 10^6$ yr while age_0 has much lower values of $10^4 – 10^6$ yr in continental margin sediments. Methane formation is further inhibited by the accumulation of dissolved metabolites (DIC and CH_4) within ambient pore fluids. Assuming typical concentrations of $C_{DIC} = C_{CH4}$ = 50 mM and an inhibition constant of K_C = 40 mM, Eq. (10) can be applied to calculate the POC fraction being converted into methane within the methanogenic zone (s. Fig. 6).

The residence time of sediments within the methanogenic zone is limited by the geothermal gradient since microbial methane formation can not proceed at temperatures above approximately 100°C. Assuming a geothermal gradient of 30 -

40°C/km, the deep biosphere may extend to a sediment depth of about 3 km. At continental margins with typical burial velocities of 10 – 100 cm kyr^{-1}, the residence time within the methanogenic zone may thus fall into a range of t = 3 to 30 million years. Fig. 6 and Eq. (10) show that about 10 – 20 % of the POC entering the methanogenic zone is microbially converted into methane under these assumptions (for $age_0 = 10^5$ yr). The residence time in deep-sea sediments is limited by the thickness of pelagic sediments and the age of the underlying oceanic crust. Adopting a typical crustal age of about 50 - 60 million years as estimate of the residence time, Eq. (10) predicts that only 9 % of the POC is converted into methane (for $age_0 = 10^7$ yr.).

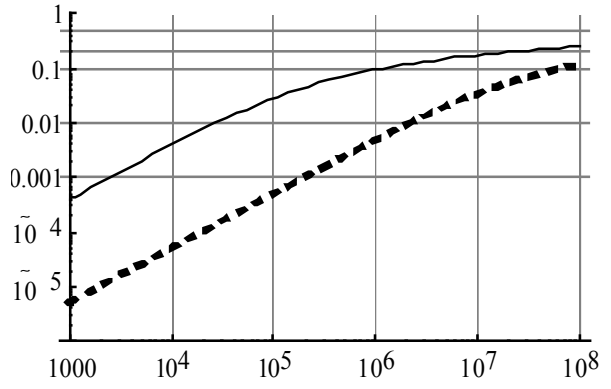

Figure 6 Fraction of POC converted into methane carbon within the methanogenic zone (f_M, y-axis) as function of residence time (t in yr, x-axis, Eq. 10). The dashed line is representative for deep-sea sediments with $age_0 = 10^7$ yr while the solid line represents continental margin sediments with $age_0 = 10^5$ yr.

Considering the arguments and equations presented above it is now possible to estimate the rate of microbial methane formation in marine sediments at global scale applying current estimates of global POC accumulation rates below the bioturbated zone [29]. The resulting time-integrated rates of methane formation are shown in Tab. 2. The global rate amounts to 70 000 Gt of methane carbon with more than 90 % of methane formation taking place at the continental margins. This number would correspond to the global inventory of biogenic methane within marine sediments if none of the methane would be lost by upward diffusion, fluid flow and gas ascent.

However, field data clearly show that a large fraction of methane is lost by upward diffusion and fluid flow into the overlying sulfate-bearing zone where methane is consumed by microbial consortia using sulfate as terminal electron acceptor [30, 31]. The biogenic methane inventory is thus certainly much smaller than the time-integrated rate of biogenic methane formation derived above. Nevertheless, the number of 70 000 Gt C is a useful upper limit for biogenic methane accumulation. Interestingly, the global methane hydrate inventory estimated by [4] approaches this upper limit value.

	F_B	F_M	I_M
Deep-sea	0.015	0.001	4 000
Margin	0.125	0.039	66 000

Table 2 Global rates of microbial methane formation in marine sediments. F_B is the POC accumulation rate below the bioturbated zone [29]. F_M gives the POC flux into the methanogenic zone assuming sulfate exposure times of 10^5 yr for the continental margin and 10^7 for pelagic sediments. F_B and F_M are given in Gt C yr^{-1}. I_M is the time-integrated rate of microbial methane formation (in Gt C) assuming POC residence times of 10^7 yr for the continental margin and 5 x 10^7 yr for deep-sea sediments.

Thickness of the gas hydrate stability zone

Methane hydrates are only stable at low temperatures and high pressures. The stability field of structure type-I methane hydrate is well defined [32]. Pitzer equations can be used to constrain the effects of seawater salinity and porewater composition on methane hydrate stability [33]. The stability field for sulfate-free seawater with a salinity of 35 PSU is shown in Fig. 7.

The upper limit of the GHSZ in marine sediments is defined by ambient water depths and bottom water temperature while the lower limit is constrained by the geothermal gradient. Data sets are available to define the upper limit at global scale. However, a global data set of geothermal gradients in marine sediments is unfortunately not available. Thus, we applied the global heat flow data set provided by the International Heat Flow Commission (IHFC) to circumvent this problem. Sediment temperatures were assumed to be in

steady-state and were computed assuming a thermal conductivity of 1.5 W m^{-1} K^{-1} [9]. The resulting global GHSZ map is shown in Fig. 8. The map shows an extended and deep-reaching GHSZ at high latitudes and around passive continental margins whereas a thin GHSZ is derived for the open ocean where the thickness of the GHSZ is limited by the thin sedimentary cover.

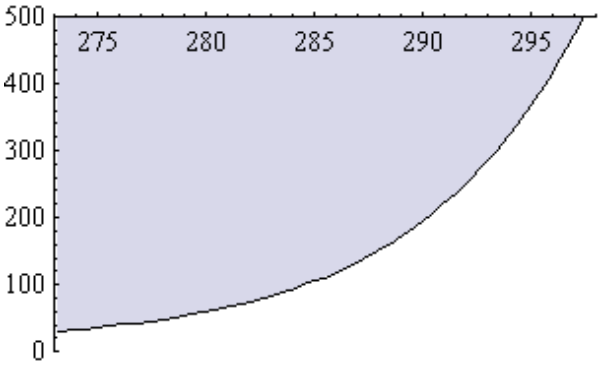

Figure 7 Stability field of type-I methane hydrate in sulfate-free seawater with a salinity of 35 PSU [33]. The x-axis is temperature in K while the y-axis gives pressure in bar. The shaded area indicates the hydrate stability field.

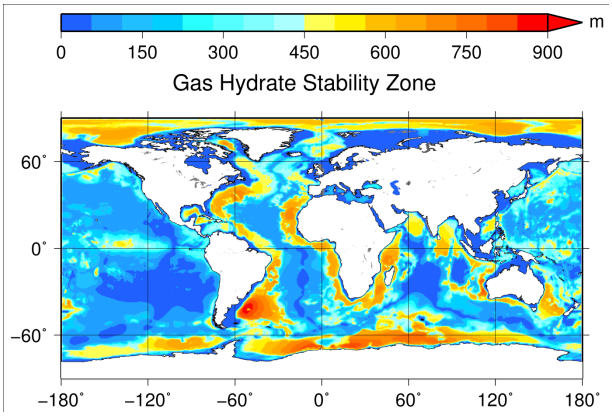

Figure 8 Thickness of the GHSZ in marine sediments calculated from global heat flow data and the hydrate stability field shown in Fig. 7 [9].

Solubility of methane hydrate in pore fluids

Gas hydrates are only formed within the GHSZ if the concentration of dissolved methane in ambient pore fluids exceeds the solubility of methane hydrate. The solubility of structure type-I methane hydrate increases with temperatures and decreases with pressure [33]. Low solubilities favoring the formation of gas hydrates are thus obtained at high pressures and low temperatures (s. Fig. 9).

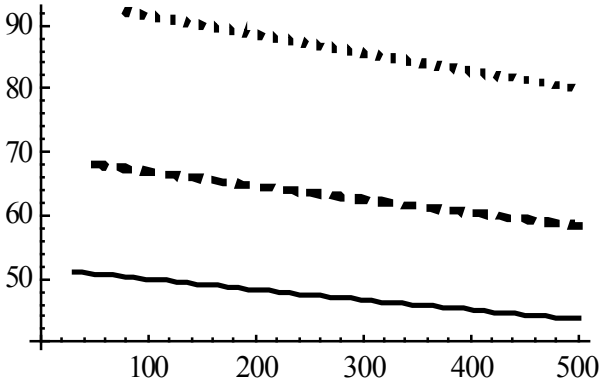

Figure 9 Solubility of type-I methane hydrate in sulfate-free pore water at S = 35 [33]. The x-axis is pressure in bar and the y-axis give the solubility of methane hydrate in mmol/kg. The solid line is valid for 0°C, the broken line indicates the solubility at 5°C and the dotted line gives the solubility at 10°C.

The thermodynamic model of [33] applied above for the calculation of methane hydrate solubility is based on the Pitzer approach and is consistent with the experimental data on methane hydrate solubility. It should, however, be noted that only a very limited set of experimental data is currently available and more work needs to be done to clearly constrain the solubility of methane hydrate in marine pore fluids.

Upward fluid flow and gas migration

Methane produced by microbial and thermal POC degradation in deep sediments underlying the GHSZ may ascend into the GHSZ where it is transformed into gas hydrate. The GHSZ may thus act as a "cold trap" for upward migrating methane. Methane can be transported as gas and in dissolved form via upward fluid flow. Numerous cold seep sites have been documented at the deep-sea floor where rich ecosystems evolve that use upward migrating methane as energy source [34-36]. Large fractions of the sedimentary pore space are saturated by gas hydrate in areas of active upward gas and fluid flow. These areas are prime targets for economic exploitation since the production rate of natural gas from marine methane hydrates is greatly enhanced at high pore space saturations.

The global rate of upward fluid flow may be estimated from a steady-state pore water budget. Sediments accumulating at the seafloor are subject

to compaction. The porosity thus decreases with increasing sediment depth (s. Fig. 10). However, a significant volume of pore water remains within the sediment after steady-state compaction.

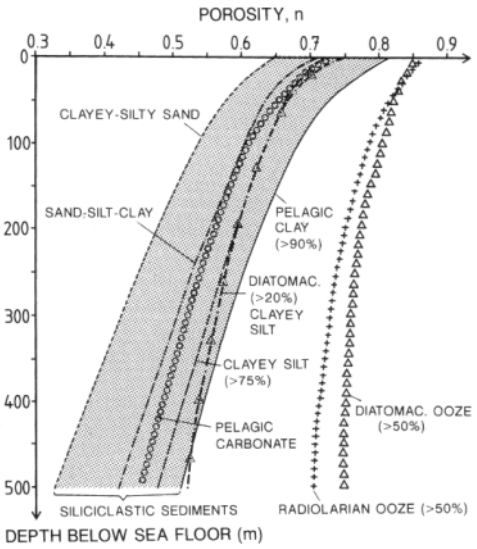

Figure 10 Down-core porosity decrease in marine sediments induced by steady-state sediment compaction [37]

The global rate of pore water burial at the seafloor after compaction (A_P in $cm^3\ yr^{-1}$) may be estimated from the global sedimentation rate (A_S = 19.6 x 10^{15} g yr^{-1}, Tab. 1), the mean density of dry solids (d_S = 2.5 g cm^{-3}) and the porosity after compaction (Φ_f = 0.1 – 0.3):

$$A_P = \frac{\Phi_f A_S}{d_S (1 - \Phi_f)} \qquad (11)$$

The resulting value of A_P = 0.9 – 3.4 $km^3\ yr^{-1}$ corresponds to independent estimates of upward fluid flow at active continental margins (1 – 2 $km^3\ yr^{-1}$, [38, 39]) indicating that most of the buried pore fluids are mobilized at continental margins by tectonic over-pressuring. The flux of dissolved methane into the GHSZ via upward fluid flow may be estimated as about 1 - 4 Tg C yr^{-1} assuming that the buried pore fluids have a mean dissolved methane concentration of 100 mM and are ascending into the GHSZ at continental margins. Over a period of 10 million years, this upward flux of methane would introduce 10 000 – 40 000 Gt of methane carbon into the GHSZ. It is thus likely that a significant fraction of the biogenic methane produced at continental margins (66 000 Gt C, Tab. 2) is ultimately transported into the GHSZ via upward fluid flow.

The fate of methane gas produced below the GHSZ is uncertain. The bottom simulating reflector (BSR) found at many continental margins is produced by the strong seismic contrast between gas below the GHSZ and gas hydrate within the GHSZ. Seismic surveys show a wide-spread occurrence of the BSR indicating that a significant fraction of methane gas is not mobile but retained and buried in sediments underlying the GHSZ. However, seismic chimneys indicating the ascent of free gas are also frequently observed at continental margins and are often associated with high gas hydrate saturations in the overlying GHSZ. It thus seems that the free gas is usually immobile but locally mobilized and transported into the GHSZ. The physical controls on gas transport into the GHSZ are poorly understood and it is currently not possible to evaluate this important transport mechanism at global scale.

Global methane hydrate inventory in marine sediments

A steady-state transport-reaction model was developed by Wallmann et al. [27] to simulate the formation of methane hydrates in marine sediments. The model considers sediment burial, compaction (s. Fig. 10), molecular diffusion, sulfate reduction, methanogenesis (Eq. 9), anaerobic oxidation of methane at the sulfate-methane transition zone and gas hydrate formation from over-saturated pore fluids (Fig. 9).

The model was applied on a global grid defined by the POC concentration data shown in Fig. 1, the burial velocities defined by Eq. 2 (Fig. 2), and the GHSZ map depicted in Fig. 8. The model did not consider the transport of methane into the GHSZ via upward gas and fluid flow. The gas hydrate formation simulated with this model run is thus only supported by the microbial methane formation within the GHSZ. Most of the methane formed within the GHSZ is lost to the overlying sediments by molecular diffusion and microbial oxidation in the sulfate-methane transition zone. The POC transfer into the methanogenic zone is limited by the low burial velocities in the GHSZ since the continental shelf acts as an efficient sediment trap under Holocene boundary conditions. The global methane hydrate inventory

in marine sediments calculated with this approach is very small (4 Gt of methane carbon, [9]).

The first model-based estimate of the global methane hydrate inventory under Holocene boundary conditions was presented by Buffett and Archer [3]. They used the POC rain rate to the seabed as a major external driving force for the simulation of hydrate formation in marine sediments. The rain rate was calculated as a function of water depth and applied as an upper boundary condition for an early diagenesis model simulating the degradation of POC in the top meter of the sediment column [40]. The POC burial rate at 1 m sediment depth calculated with this "muds" model was applied as upper boundary condition for the simulation of methane turnover in the underlying sediment sequence. The later simulations consider the microbial degradation of POC via sulfate reduction and methanogenesis and the anaerobic oxidation of methane within the sulfate-methane transition zone [41, 42]. POC was separated into an inert fraction and a labile fraction that was degraded over the top km of the sediment column following first order reaction kinetics (rate constant 3 x 10^{-13} s^{-1}). The model also considers an externally imposed rate of upward fluid flow. It was calibrated using field data obtained at Blake Ridge (a passive margin site) and the Cascadia margin (active continental margin). The best fit to observations was obtained assuming that the 25 % of the total POC is labile and using upward fluid flow velocities of 0.23 mm yr^{-1} (passive margin) to 0.4 mm yr^{-1} (active margin). Applying these parameter values on a global grid and assuming a compensating downward fluid flow over 50 % of the global seafloor area resulted in a total methane hydrate inventory of 3000 Gt C [3]. The hydrate inventory was to a large degree controlled by the velocity of upward fluid flow that was assumed to exceed the flow rate induced by sediment compaction by 20 % (passive margins) to 60 % (active margins). Without imposed fluid flow, the global hydrate inventory was reduced to 600 Gt C [3]. Subsequently, the authors discovered an extrapolation error in the calculation of POC rain rates as function of water depth [5]. The model-based estimate of the global hydrate inventory was reduced from 3000 Gt C to approximately 700 – 900 Gt C after correction for this error [5]. Even after this downward revision, the calculated hydrate inventory is still two orders of magnitude higher than the Holocene inventory calculated by us [9]. This difference is probably caused by the neglect of upward fluid flow in our model. It seems that most of the gas hydrate formation is caused by methane migration under Holocene boundary conditions.

Klauda and Sandler [4] used a slightly modified version of the Davie and Buffett model [42] to estimate the global marine hydrate inventory. The entire POC pool was assumed to be completely degradable with a reduced decay constant of 1.5 x 10^{-14} s^{-1}. The upper boundary of the model domain was constrained by field data. POC concentrations measured in surface sediments and Holocene sedimentation rates averaged over the major ocean basins were applied to define the POC burial flux at the sediment surface [4]. The global hydrate inventory estimated with this approach was surprisingly high (57 000 Gt C) even though the model was run without imposing upward fluid flow. Unfortunately, Klauda and Sandler [4] did not consider POC degradation via sulfate reduction. The large difference to our estimate may be explained by the neglect of microbial sulfate reduction and methane oxidation since the accumulation of methane in pore fluids and gas hydrates is strongly diminished by these processes. Moreover, Buffett and Archer [3] and Klauda and Sandler [4] applied a lower solubility of methane hydrate than predicted by our model (Fig. 9). The reduced hydrate solubility favors hydrate formation and may account for some of the difference between ours and the previous estimates. Finally, the gas hydrate inventory is further reduced in our model by the strong down-core decrease in POC reactivity. This important kinetic factor was not considered in the previous model-based estimates. Overall, it may be concluded that gas hydrate formation via microbial methane formation within the GHSZ is very limited under Holocene boundary conditions.

In a second model run, we simulated hydrate formation under Quaternary boundary conditions. We used the same input parameter values as before but enhanced the burial velocity at the continental slope and rise by a factor of five assuming that shelf sediments are eroded and re-deposited at large water depth during glacial sea-level low-stands [9]. Under these conditions, the model predicts a global hydrate inventory of 995 Gt C. The model run confirms that the accumulation rate of gas hydrates is to a large

degree controlled by the burial velocity and the input of POC into the methanogenic zone. Most of the hydrates are found at highly productive continental margins and at high latitudes (s. Fig. 11).

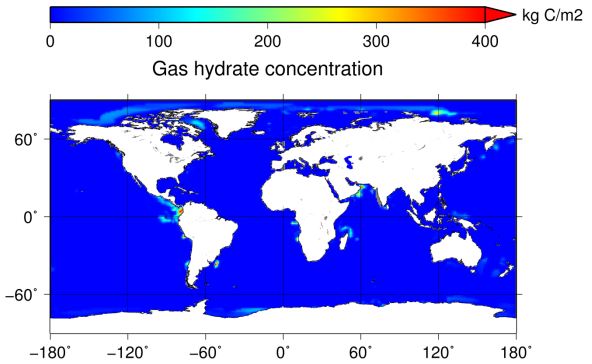

Figure 11 Global distribution of methane hydrate produced by microbial methane formation within the GHSZ under Quaternary boundary conditions [9].

It takes several million years to accumulate gas hydrates via microbial POC degradation within the GHSZ (s. Fig. 6). The Quaternary model run is thus more appropriate than the previous model runs for Holocene boundary conditions. It considers that up to 90 % of the shelf sediments accumulating during interglacial are eroded and re-deposited at the slope and rise during glacial conditions [43]. The inventory of 995 Gt C obtained in the Quaternary model run should be regarded as a minimum estimate since hydrate formation via methane ascent from deeper sediment layers is not included in this number.

The effect of upward fluid flow on gas hydrate accumulation was further investigated applying our transport-reaction model [27] with various upward fluid flow velocities prescribed at the lower boundary of the model column [44]. This modeling exercise clearly showed that the gas hydrate inventory increases dramatically by imposing an externally driven infiltration of methane-saturated fluids into the GHSZ (s. Fig. 12). The effect is most pronounced at low to moderately high POC accumulation rates.

Finally, the model was applied on the previously defined global grid to calculate the total global hydrate inventory under Quaternary boundary conditions. The global pore water balance (Eq. 11) was used to constrain the range of upward fluid flow velocities (v) at continental margins as v = 0.05 mm yr^{-1} for passive margins and 0.3 mm yr^{-1} for active margins. The global hydrate inventory estimated with this approach is 3500 Gt C (s. Fig. 13).

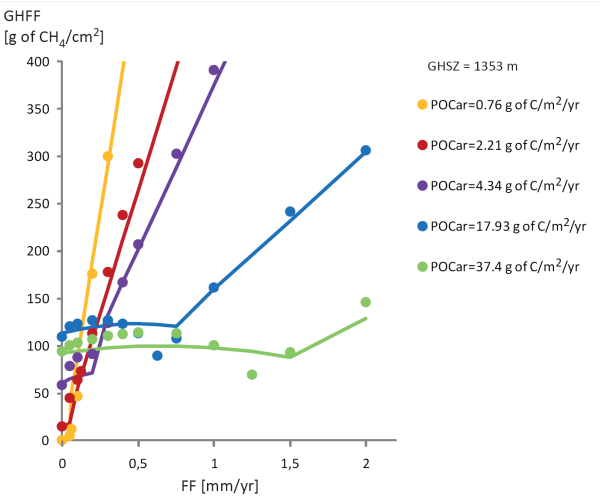

Figure 12 Effect of upward fluid flow velocity (FF) on gas hydrate accumulation for various POC accumulation rates (POCar)

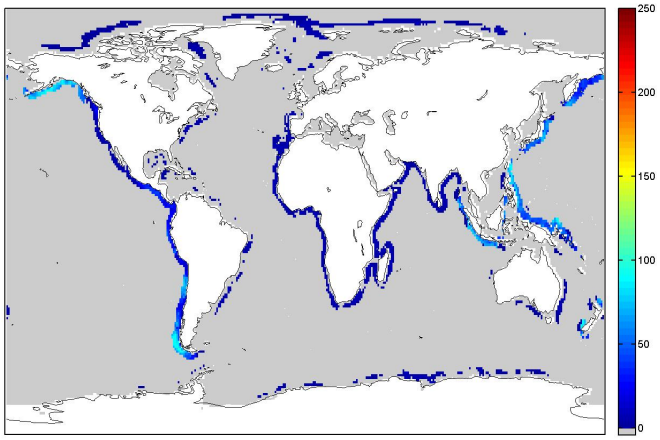

Figure 13 Global distribution of gas hydrates in marine sediments considering microbial methane formation and tectonically driven upward fluid flow [44]. The color bar indicates the depth-integrated methane hydrate inventory in g C cm^{-2}.

The model run with fluid flow predicts gas hydrate occurrences at almost all continental margins. The true distribution of gas hydrates is certainly more patchy than the distribution shown in Fig. 13 since fluids usually ascend through narrow high-permeability conduits such as faults and fractures. This focusing of upward fluid flow was not

considered in the global model. It may also affect the global estimate due to the non-linear dependency of the gas hydrate inventory on fluid flow velocity (s. Fig. 12). It should also be noted that steady-state conditions were applied in all model runs [3-5, 9, 44]. The models were run over a period of typically more than one million years until the depth-integrated inventory of gas hydrates reached a constant value. It was assumed that geothermal gradients and POC accumulation rates at the seafloor have been constant over the entire model period. Thus, the model runs do not consider subsidence, thermal evolution and the changes in POC accumulation during basin formation. Finally, the ascent of methane gas was not considered in the model runs. Significant amounts of gas hydrate may be formed by this additional methane flux into the GHSZ. Considering all the uncertainties and gaps in the available data and the limitations of the existing models, our best estimate of the global gas hydrate inventory in marine sediments is 3000 ± 2000 Gt of methane carbon.

Conclusions and outlook

We present new estimates of the global abundance of gas hydrates in marine sediments applying improved estimates of POC accumulation (Figs. 1 and 2), microbial methane formation (Fig. 6), GHSZ thickness (Fig. 8) and gas hydrate solubility (Fig. 9). Our transport reaction model shows that the microbial degradation of POC within the GHSZ produces only very small amounts of methane hydrate (4 Gt C) under Holocene boundary conditions since sediments are trapped at the continental shelf and methane is lost via upward diffusion and microbial oxidation. The global gas hydrate inventory increases to about 1000 Gt C under Quaternary boundary conditions considering that shelf sediments were eroded and re-deposited within the GHSZ under glacial conditions (Fig. 11). A further increase to 3500 Gt C is obtaining by considering upward fluid flow induced by tectonic over-pressuring at continental margins (s. Fig. 13). Allowing for additional methane input to the GHSZ via the ascent of free methane gas, our up-dated best estimate of the global methane hydrate inventory in marine sediments is 3000 ± 2000 Gt C.

The gas hydrate distributions shown in Fig. 13 may be used for prospection purposes. It should, however, be noted that detailed local surveys will almost certainly reveal inventories differing considerably form the predicted values since the regional basin evolution and the local pathways for fluid and gas flow are not resolved in our global estimates. Seismic surveys and drilling data are needed to constrain local gas hydrate inventories. Moreover, new 3-D basin modeling tools have recently been developed that can be used to better constrain gas hydrate inventories in well characterized sedimentary basins [45].

Our new estimate of the total marine gas hydrate inventory (3000 ± 2000 Gt C) implies that future seafloor warming may ultimately induce large and persistent methane emissions at the seafloor. Past hydrate inventories were probably smaller than today due to reduced sedimentation rates during the early Cenozoic and Mesozoic (s. Fig.3) and elevated bottom water temperatures. Some of the negative carbon isotopic excursions observed in the geological record were thus probably not caused by massive gas hydrate dissociation events but rather by other processes such as the intrusion of volcanic silts into POC-rich sedimentary strata.

References

1. Kvenvolden, K.A. and T.D. Lorenson, *The global occurrence of natural gas hydrate.* Geophysical Monograph, 2001. **124**: p. 87-98.
2. Milkov, A.V., *Global estimates of hydrate-bound gas in marine sediments: how much is really out there?* Earth Science Reviews, 2004. **66**(3-4): p. 183-197.
3. Buffett, B. and D. Archer, *Global inventory of methane clathrate: sensitivity to changes in the deep ocean.* Earth and Planetary Science Letters, 2004. **227**: p. 185-199.
4. Klauda, J.B. and S.I. Sandler, *Global Distribution of Methane Hydrate in Ocean Sediment.* Energy & Fuels, 2005. **19**: p. 459-470.
5. Archer, D., B. Buffett, and V. Brovkin, *Ocean methane hydrates as a slow tipping point in the global carbon cycle.* Proceedings of the National Academy of Sciences., 2008. **106**(49): p. 20596-20601.
6. Marquardt, M., et al., *A transfer function for the prediction of gas hydrate inventories in marine sediments.* Biogeosciences, 2010. **7**: p. 2925–2941.
7. Seiter, K., et al., *Organic carbon content in surface sediments - defining regional provinces.* Deep-Sea Research I, 2004. **51**: p. 2001-2026.
8. Romankevich, E.A., A.A. Vetrov, and V.I. Peresypkin, *Organic matter of the World Ocean.*

Russian Geology and Geophysics, 2009. **50**: p. 299-307.
9. Burwicz, E.B., L.H. Rüpke, and K. Wallmann, *Estimation of the global amount of submarine gas hydrates formed via microbial methane formation based on numerical reaction-transport modeling and a novel parameterization of Holocene sedimentation.* Geochimica et Cosmochimica Acta, submitted.
10. Betts, J.N. and H.D. Holland, *The oxygen content of ocean bottom waters, the burial efficiency of organic carbon, and the regulation of atmospheric oxygen.* Palaeogeography, Palaeoclimatology, Palaeoecology, 1991. **97**: p. 5-18.
11. Colman, A.S. and H.D. Holland, *The global diagenetic flux of phosphorus from marine sediments to the oceans: Redox sensitivity and the control of atmospheric oxygen levels*, in *Marine Authigenesis: From Global to Microbial*. 2000, Society of Sedimentary Geology.
12. Syvitski, J.P.M., et al., *Impact of humans on the flux of terrestrial sediment to the global coastal ocean.* Science, 2005. **308**: p. 376-380.
13. Raiswell, R., et al., *Contributions from glacially derived sediment to the global iron (oxyhydr)oxide cycle: Implications for iron delivery to the oceans.* Geochim Cosmochim Acta, 2006. **70**: p. 2765-2780.
14. Jickells, T.D., et al., *Global iron connections between desert dust, ocean biogeochemistry, and climate.* Science, 2005. **308**: p. 67-71.
15. Kleypas, J.A., *Modeled estimates of global reef habitat and carbonate production since the last glacial maximum.* Paleoceanogr., 1997. **12**(4): p. 533-545.
16. Archer, D.E., *An atlas of the distribution of calcium carbonate in sediments of the deep sea.* Global Biogeochemical Cycles, 1996. **10**(1): p. 159-174.
17. Sarmiento, J.L. and N. Gruber, *Ocean Biogeochemical Cycles.* 2006, Princeton: Princeton University Press. 503.
18. Menard, H.W. and S.M. Smith, *Hypsometry of ocean basin provinces.* Journal of Geophysical Research, 1966. **71**(18): p. 4305-4325.
19. Baturin, G.N., *Issue of the relationship between primary productivity of organic carbon in ocean and phosphate accumulation (Holocene - Late Jurassic).* Lithology and Mineral Resources, 2007. **42**(4): p. 318-348.
20. Wallmann, K., *Controls on Cretaceous and Cenozoic evolution of seawater composition, atmospheric CO_2 and climate.* Geochimica et Cosmochimica Acta, 2001. **65**(18): p. 3005-3025.
21. Devol, A.H. and H.E. Hartnett, *Role of the oxygen-deficiency zone in transfer of organic carbon to th deep ocean.* Limnol. Oceanogr., 2001. **46**(7): p. 1684-1690.
22. Hartnett, H.E. and A.H. Devol, *Role of a strong oxygen-deficient zone in the preservation and degradation of organic matter: A carbon budget for the continental margin of northwest Mexico and Washington State.* Geochimica et Cosmochimica Acta, 2003. **67**(2): p. 247-264.
23. Berelson, W.M., et al., *Biogenic matter diagenesis on the sea floor: A comparison between two continental margin transects.* Journal of Marine Research, 1996. **54**: p. 731-762.
24. Reimers, C.E., R.A. Jahnke, and D.C. McCorkle, *Carbon fluxes and burial rates over the continental slope and rise off Central California with implications for the global carbon cycle.* Global Biogeochemical Cycles, 1992. **6**(2): p. 199-224.
25. Seiter, K., C. Hensen, and M. Zabel, *Benthic carbon mineralization on a global scale.* Global Biogeochemical Cycles, 2005. **19**(GB1010): p. doi:10.1029/2004GB002225.
26. Flögel, S., et al., *Simulating the biogeochemical effects of volcanic CO2 degassing on the oxygen-state of the deep ocean during the Cenomanian/Turonian Anoxic Event (OAE2).* Earth and Planetary Science Letters, in press.
27. Wallmann, K., et al., *Kinetics of organic matter degradation, microbial methane generation, and gas hydrate formation in anoxic marine sediments.* Geochim. Cosmochim. Acta, 2006. **70**: p. 3905-3927.
28. Middelburg, J.J., *A simple model for organic matter decomposition in marine sediments.* Geochimica et Cosmochimica Acta, 1989. **53**: p. 1577-1581.
29. Wallmann, K., *Phosphorus imbalance in the global ocean?* Global Biogeochemical Cycles, 2010. **24**: p. doi:10.1029/2009GB003643.
30. Borowski, W.S. and C.K. Paull, *Marine pore-water sulfate profiles indicate in situ methane flux from underlying gas hydrate.* Geology, 1996. **24**(7): p. 655-658.
31. Luff, R. and K. Wallmann, *Fluid flow, methane fluxes, carbonate precipitation and biogeochemical turnover in gas hydrate-bearing sediments at Hydrate Ridge, Cascadia Margin: Numerical modeling and mass balances.*

Geochimica et Cosmochimica Acta, 2003. **67**(18): p. 3403-3421.
32. Sloan Jr., E.D., *Clathrate Hydrates of Natural Gases*. Second ed. Chemical Industries, ed. H. Heinemann. 1998, New York: Marcel Dekker, Inc. 705.
33. Tishchenko, P., et al., *Calculation of the stability and solubility of methane hydrate in seawater.* Chemical Geology, 2005. **219**: p. 37-52.
34. Suess, E., et al., *Biological communities at vent sites along the subduction zone off Oregon*, in *The Hydrothermal Vents of the Eastern Pacific: An Overview*, M.L. Jones, Editor. 1985, Bull. Biol. Soc. Wash. p. 475-484.
35. Suess, E., et al., *Gas hydrate destabilization: Enhanced dewatering, benthic material turnover and large methane plumes at the Cascadia convergent margin.* Earth and Planetary Science Letters, 1999. **170**: p. 1-15.
36. Wallmann, K., et al., *Quantifying fluid flow, solute mixing, and biogeochemical turnover at cold vents of the eastern Aleutian subduction zone.* Geochimica et Cosmochimica Acta, 1997. **61**(24): p. 5209-5219.
37. Einsele, G., *Sedimentary Basins: Evolution, Facies, and Sediment Budget*. Second ed. 2000, Berlin: Springer. 792.
38. Von Huene, R. and D.W. Scholl, *Observations at convergent margins concerning sediment subduction, subduction erosion, and the growth of continental crust.* Rev. Geophys., 1991. **29**(3): p. 279-316.
39. Moore, J.C. and P. Vrolijk, *Fluids in accretionary prisms*. Rev. Geophys., 1992. **30**: p. 113-135.
40. Archer, D.E., J.L. Morford, and S.R. Emerson, *A model of suboxic sedimentary diagenesis suitable for automatic tuning and gridded global domains*. Global Biogeochemical Cycles, 2002. **16**(1): p. 10.1029/2000GB001288.
41. Davie, M.K. and B.A. Buffett, *A numerical model for the formation of gas hydrate below the seafloor.* Journal of Geophysical Research, 2001. **106**(B1): p. 497-514.
42. Davie, M.K. and B.A. Buffett, *A steady state model for marine hydrate formation: Constraints on methane supply from pore water sulfate profiles.* Journal of Geophysical Research, 2003. **108**(B10): p. 2495, doi:10.1029/2002JB002300.
43. Hay, W.W., *Pleistocene-Holocene Fluxes Are Not the Earth's Norm*, in *Material Fluxes on the Surface of the Earth*, W.W. Hay and T. Usselman, Editors. 1994, National Academy Press: Washington. p. 15-27.
44. Piñero, E., et al., *Effect of in situ methane formation and fluid advection on the global gas hydrate distribution in marine sediments.* In preparation.
45. Piñero, E., et al. *3-D numerical modeling of methane hydrate deposits. Proceedings of the 7th International Conference on Gas Hydrates.* 2011. Edinburgh, Scotland, United Kingdom.

Acknowledgements
This work was funded by the German national gas hydrate project SUGAR and the Kiel-based Cluster of Excellence “The Future Ocean”.